Ocean Systems Engineering, *Vol. 16, No. 1 (2026) 63-81*
https://doi.org/10.12989/ose.2026.16.1.063

Techno-Press

Experimental evaluation of serviceability of multi-unit floating structures with wave-dissipating modules

Youn-Ju Jeong*[1], Min-Su Park[1a], Young-Taek Kim[2b], Jeongsoo Kim[1c]

[1]*Department of structural engineering research, Korea Institute of Civil Engineering and Building Technology, 283 Goyangdae-ro, Goyang, Gyeonggi-Do,10223, South Korea*
[2]*Department of hydro science & engineering research, Korea Institute of Civil Engineering and Building Technology, 283 Goyangdae-ro, Goyang, Gyeonggi-Do,10223, South Korea*

(Received January 21, 2026, Revised March 5, 2026, Accepted March 7, 2026)

Abstract. This study experimentally evaluated the serviceability of multi-unit floating structures designed for marine city applications and verified the effect of wave-dissipating modules on wave motion reduction. Serviceability indicators were defined as vertical acceleration and inclination (pitch and roll), reflecting both the stable operation of topside facilities and human activity and discomfort (motion sickness). The experimental results showed that the installation of wave-dissipating modules reduced vertical RMS accelerations by approximately 34-39% and pitch/roll inclinations by 21-42%. These improvements were consistently observed not only under 1-year return period wave conditions but also under extreme 100-year return period waves, thereby confirming the reliability of the proposed design. This study demonstrates that wave-dissipating modules are an effective design strategy to enhance the habitability and serviceability of floating infrastructures for marine cities. Furthermore, it highlights the need to extend conventional serviceability evaluation frameworks, which have been focused on industrial facilities, to ergonomics-based criteria that reflect the dual requirements of technical stability and human-oriented serviceability in marine city environments. These findings are expected to make an important contribution to the development of next-generation offshore infrastructures, such as marine cities and offshore renewable energy hubs, where both technical stability and human-oriented serviceability must be simultaneously ensured.

Keywords: acceleration; floating structure; inclination; marine city; motion reduction; serviceability; wave-dissipating module

1. Introduction

Recently, there has been a growing interest and demand for the eco-friendly utilization of maritime space through floating offshore infrastructure. Such infrastructure can be broadly classified into two categories: industrial facilities such as plants and ports, and human-oriented facilities such as marine cities. Traditionally, floating infrastructure has been widely applied to industrial purposes, including container ports and energy storage platforms for oil and LNG.

*Corresponding author, Ph.D., E-mail: yjjeong@kict.re.kr
[a] Ph.D., E-mail: mspark@kict.re.kr
[b] Ph.D., E-mail: ytkim@kict.re.kr
[c] Ph.D., E-mail: jeongsookim@kict.re.kr

http://www.techno-press.org/ose/5
ISSN: 2093-6702 (Print), 2093-677X (Online)

However, in recent years, projects aimed at human habitation have begun to emerge, such as the Oceanix Project in Busan, South Korea, and the NEOM City (Oxagon) project in Saudi Arabia. In addition, initiatives such as Denmark's Net-zero Race Project seek to construct renewable energy hubs within offshore wind farms to address the intermittency of renewable energy output. These trends indicate that the operational conditions of floating infrastructure are gradually shifting toward "manned conditions". Accordingly, from the perspective of motion performance, floating structures must satisfy performance requirements that reflect this recent trend.

The serviceability of floating infrastructure can be defined as the ability to control wave-induced motions of the floating body to a level that ensures the intended functionality of the topside facilities. For industrial-purpose floating infrastructure, serviceability guidelines have primarily focused on pitch and roll angle criteria to secure stable operation of the topside facilities, mainly to prevent equipment malfunction or failure [1-5]. In contrast, for marine cities intended for human habitation and activity, serviceability guidelines emphasize vertical acceleration criteria to prevent motion sickness and ensure human comfort and activity [2, 4, 6-8], as presented in Fig. 1. From an ergonomic perspective, such serviceability guidelines are being extended not only to marine cities but also to offshore industrial facilities such as floating wind farms, where they address the health and safety of maintenance personnel [2, 7, 8].

At RWTH Aachen University, serviceability guidelines applicable to maintenance personnel on floating offshore wind platforms were investigated [8]. It was reported that serviceability guidelines addressing human discomfort (motion sickness) must include the low-frequency range (0.1-0.5 Hz) and vertical acceleration term, and therefore ISO 2631-1:1997 was deemed appropriate [8]. In addition, although Nordforsk guideline [4] provides guidelines originally intended for ships, it has been widely cited in the marine industry and is considered a useful reference. The Nordforsk guidelines [4] classify serviceability criteria for human activity (workability) on ships-based on acceleration and inclination-into five groups.

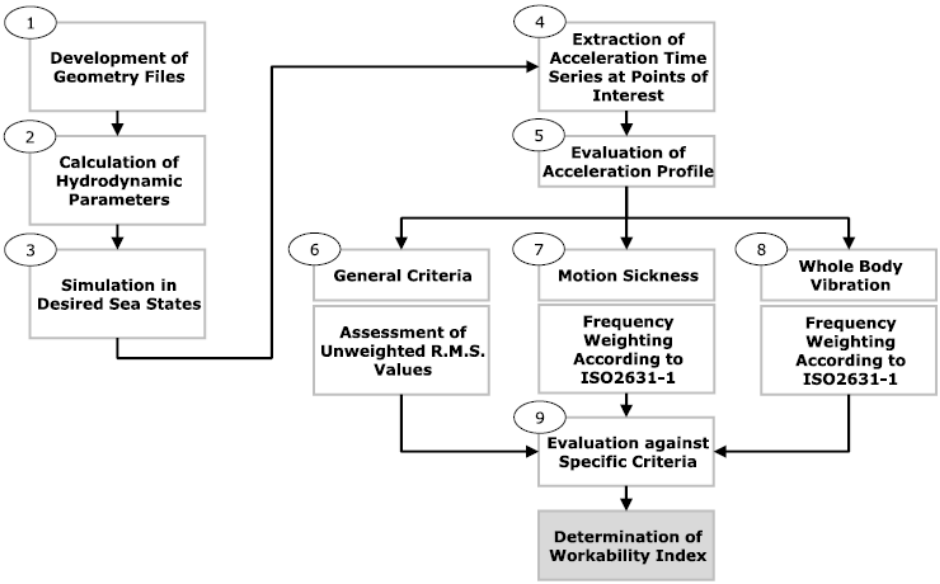

Figure 1. Methodology for accessing motions on floating offshore wind turbines

Marjanen [9] studied validation methods for the guidelines specified in ISO 2631-1:1997 [6] with respect to human motion sickness in multi-axial vibration environments. Scheu et al. [7] utilized ISO 2631-1:1997 to develop a workability index for personnel operating on floating offshore wind platforms according to the process presented in Fig. 1. Fang and Chan [10] applied the methods of ISO 2631-1:1997 to investigate vertical motion sickness in high-speed ferries, reporting that numerical analysis results may show some discrepancies in the pitch resonance region.

Kim et al. [11] explored the use of Analysis Wavelet Transform (AWT) as an alternative to the commonly used FFT method in the time-frequency conversion process for calculating frequency-weighted RMS acceleration. Asua et al. [12] evaluated passenger discomfort and motion sickness in vehicles using the frequency-weighted RMS acceleration index specified in ISO 2631. Sindre [13] evaluated the location-specific serviceability on the feed barge and conducted a comparative analysis against serviceability guidelines. Furthermore, Jeong et al. [2] conducted a serviceability assessment of floating infrastructure using ISO 2631-1:1997 based on wave flume (2D) tests. However, since the experiments were limited to half the beam width of the floating body in a 2D wave flume, the results did not fully reflect the serviceability of actual models subjected to multi-axial environments.

In this study, an experimental serviceability assessment was conducted through wave basin (3D) tests on a multi-unit floating infrastructure (4×2 EA array) designed for marine cities. In addition, the serviceability improvement effect was compared and analyzed between the prototype model and the case in which wave-dissipating modules were installed around the periphery to reduce the wave-induced motions of the main floating body. Based on the two experimental cases, serviceability indicators of the floating body-namely vertical acceleration and inclination angles (pitch and roll)-were evaluated and compared.

2. Small scale tests

2.1 Test models and set-up

2.1.1 Test models

To experimentally evaluate the serviceability of multi-unit floating structures, wave basin (3D) tests were conducted. The test model was designed based on the marine city concept shown in Fig. 2, applying a Froude scale ratio of 1/60, and constructed as a 4×2 units array (total of 8 units). In addition, wave basin tests were also performed to verify the serviceability improvement effect when wave-dissipating modules were installed to reduce the wave-induced motions of the main floating body. The detailed specifications of the test model are presented in Table 1.

For unit-to-unit connections of the floating body, a fender-cable connection method was adopted to ensure flexible joint behavior while maintaining uniform motion among the units, as shown in Fig. 3. Specifically, three types of cables (two lateral and one diagonal-vertical) were used to connect the units. In this method, the fender resists compressive forces between units, while the cables resist tensile forces (separating forces), thereby stabilizing the behavior of the connections. Regarding the mooring system, since the marine city is intended to be located in coastal areas with mild sea conditions and water depths of approximately 20 m, a dolphin-fender mooring system (10 units in total) was applied. This method is suitable for such conditions and minimizes the wave-induced motions of the floating body.

The wave-dissipating module consists of external slits, which dissipate wave energy acting on the floating body, and internal buoyancy cells, which provide the module's own buoyancy, as shown in Fig. 4. To enhance wave energy dissipation, vertical slits [14, 15] with a porosity of 30% [2, 16, 17] were applied to both the front and rear walls. The internal buoyancy cells were designed in the form of circular columns, and together with the slit walls at the front and rear, they form a semi-double chamber configuration [18-20]. Furthermore, the bottom plate of the wave-dissipating module was devised to partially function as a heave plate [21-29]. The peripheral wave-dissipating modules were fabricated with the same draft and freeboard as the main floating body, and rigid connections using steel rods were applied between the modules and the main structure. As shown in Table 2, the experimental models were classified into two cases depending on whether the wave-dissipating modules were installed.

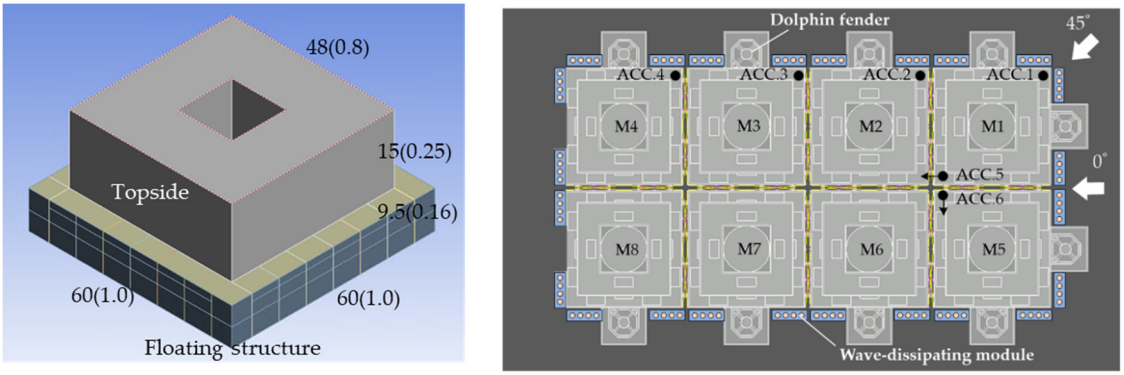

(a) 1 unit (m) (b) 4×2 units array

Figure 2. Test model

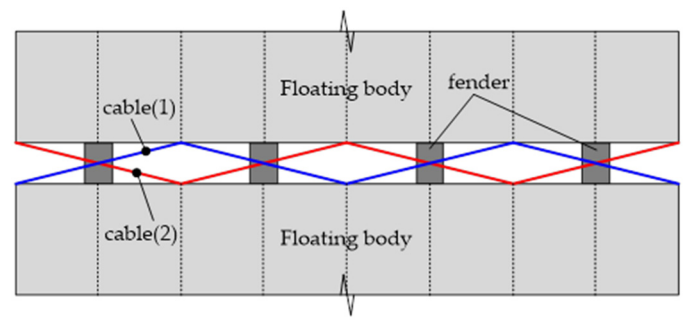

(a) Plan view

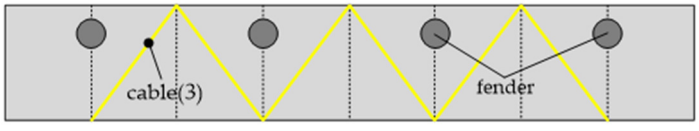

(b) Front view

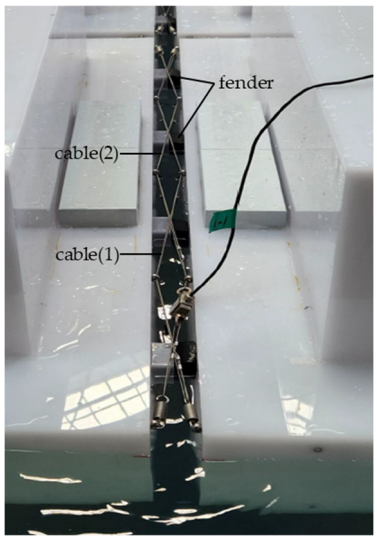

(c) Install

Figure 3. Fender-cable connection (unit-unit) details

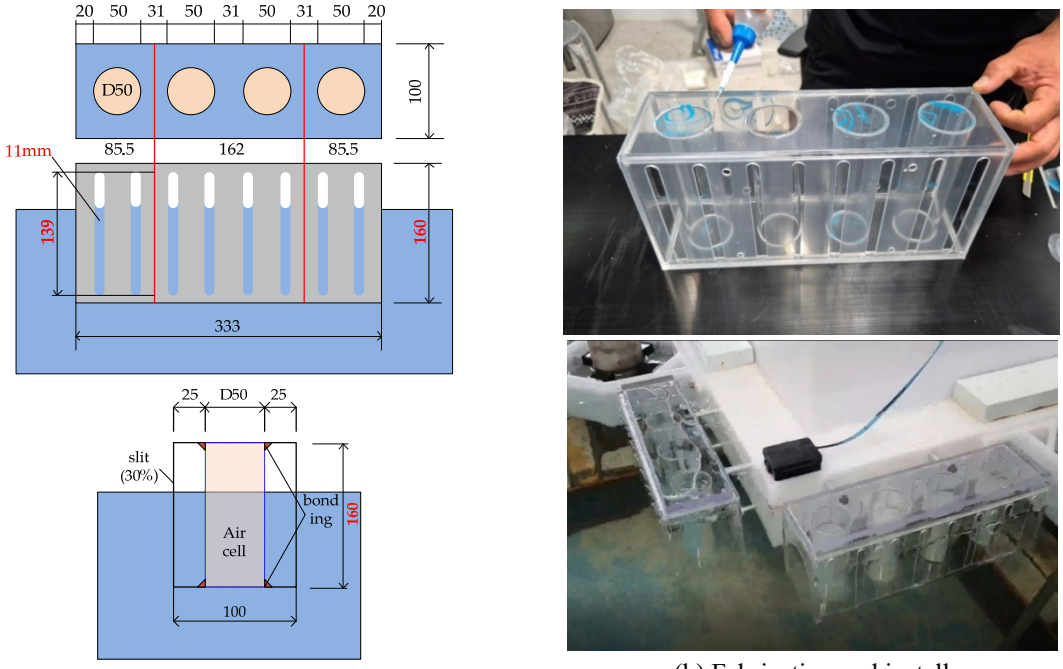

(a) Details

(b) Fabrication and install

Figure 4. Wave-dissipating module

Table 1. Dimension of test models

Items	Dimension(m) (L×W×H)	Weight (kg)	Etc.
1. Floating structure	1.00×1.00×0.16	64.80	-
2. Topside	0.80×0.80×0.25	50.46	-
3. Wave dissipating modules	0.33×0.10×0.16	1.28	1EA

Table 2. Test model cases

Cases	Test models		
	Floating structure	Topside building	Wave-dissipating module
CASE 1	○	○	-
CASE 2	○	○	○

2.1.2 Set-up and measurement

The experimental setup of the test model in the 3D wave basin is shown in Fig. 5. The purpose of this experiment was to evaluate serviceability indicators by measuring the wave-induced motions of the multi-unit floating structure. To accurately capture the motions of the eight floating units, a motion capture system employing ultraviolet cameras was utilized. In addition, as shown in Fig. 2(b), six accelerometers were installed at the corners of the floating body for supplementary measurements.

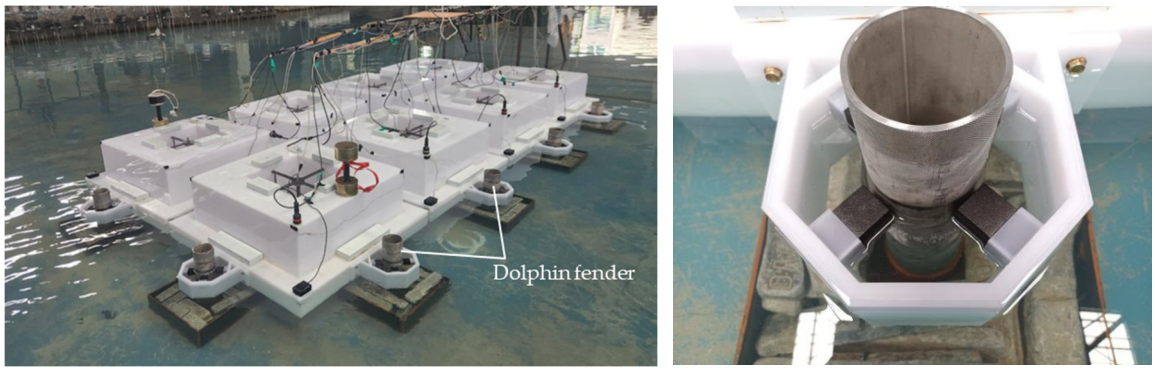

(a) Test model installation (b) Dolphin-fender mooring

Figure 5. Test model set-up

Table 3. Wave conditions (irregular, JONSWAP γ=3.3)

No.	T_p (s.) Small (real)	H_s (cm) Small (real)	Return period
IR-1	0.65 (5.0)	2.17 (130)	
IR-2	0.71 (5.5)	2.17 (130)	1 yr.
IR-3	0.84 (6.5)	2.17 (130)	
IR-4	0.71 (5.5)	3.33 (200)	
IR-6	0.84 (6.5)	3.33 (200)	
IR-7	0.90 (7.0)	3.33 (200)	100 yr.
IR-8	0.97 (7.5)	3.33 (200)	

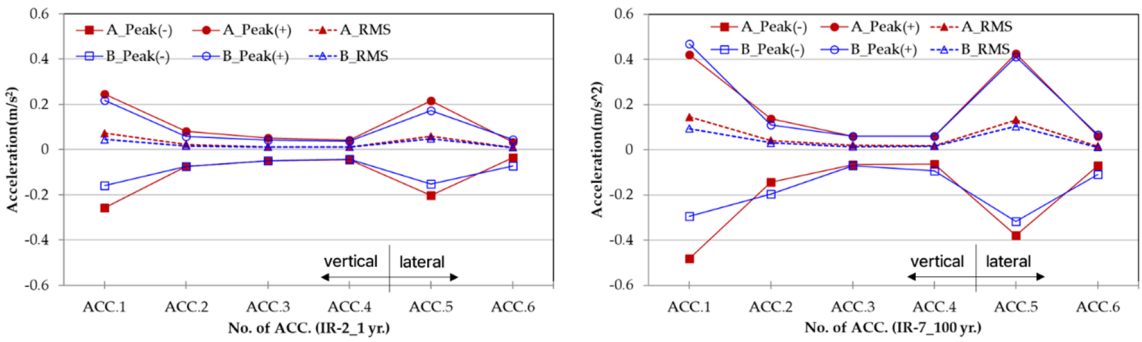

(a) Incident wave 0˚ (1 yr.) (b) Incident wave 0˚ (100 yr.)

Figure 6. Vertical acceleration distribution

2.1.3 Waves conditions

Irregular wave loads corresponding to return periods of 1 year and 100 years were applied as design conditions, as summarized in Table 3. The purpose of evaluating the wave-induced motions of the floating body was to assess its serviceability, and many projects and guidelines related to

serviceability adopt evaluations based on 1-year return period waves [2]. Accordingly, in this study, wave basin tests were primarily conducted under 1-year return period conditions. Additionally, to investigate the effectiveness of wave-dissipating modules in reducing wave-induced motions under extreme conditions, supplementary experiments were performed using 100-year return period waves. The water depth was set to 20 m.

3. Evaluation of serviceability indicators

To determine the serviceability evaluation positions of the multi-unit floating body [13], the distributions of vertical acceleration and inclination for each unit, as shown in Fig. 2(b), were analyzed (Fig. 6 and Fig. 7). Based on this analysis, the M1 unit (maximum value) and the M3 unit (minimum value) were selected as representative positions for serviceability evaluation with

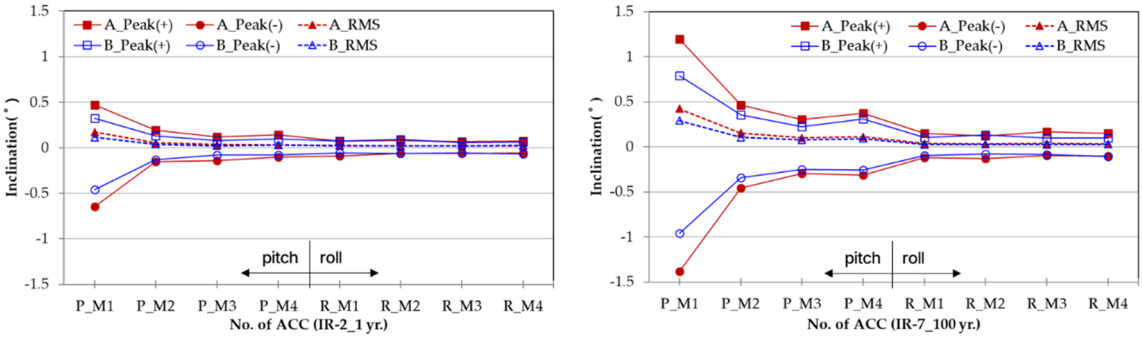

(a) Incident wave 0° (1 yr.) (b) Incident wave 0° (100 yr.)

Figure 7. Inclination distribution

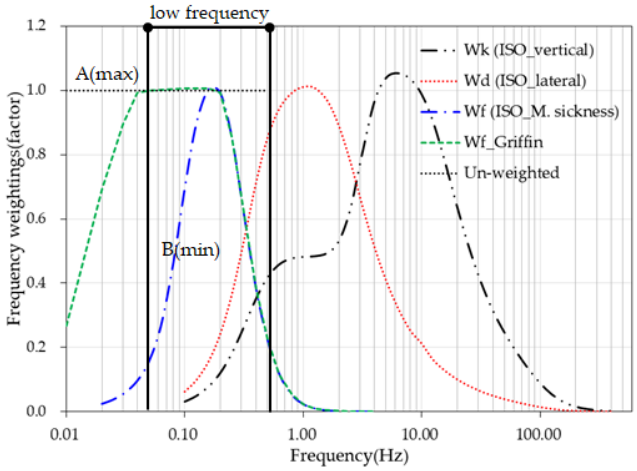

Figure 8. Frequency-weighting function to motion sickness (W_f)

respect to wave-induced motions. Although various wave loads were applied in the wave basin tests to investigate motion characteristics, only the 1-year return period wave load (IR-2) and the 100-year return period wave load (IR-7) were utilized for serviceability evaluation.

3.1 Vertical acceleration

The serviceability evaluation indicator for vertical acceleration was assessed by calculating the RMS values from time-history data. Here, the RMS values include both the un-weighted RMS acceleration, which serves as a general indicator of human activity [4], and the frequency-weighted RMS acceleration, which serves as an indicator of motion sickness [2, 6, 7]. The concept of frequency weighting reflects the sensitivity of human motion sickness to different frequency ranges by applying differentiated weighting factors to the motion amplitudes in each frequency band. To this end, as shown in Fig. 8, ISO 2631-1:1997 [6] provides a frequency weighting function (W_f) for human motion sickness. Accordingly, as shown in Fig. 9, the frequency-weighted amplitude is obtained by multiplying the amplitude of the frequency-domain response spectrum-derived from FFT of the vertical acceleration time history-by the weighting function (W_f). The inverse FFT of this frequency-weighted amplitude then yields the time-history data, from which the RMS value is calculated to determine the frequency-weighted RMS acceleration [2, 9, 11].

At the serviceability evaluation position, M1 unit (ACC.1), the vertical acceleration time-history data measured for Models A and B are shown in Fig. 10 and Fig. 11, respectively. The frequency-domain response spectrum obtained through FFT of the vertical acceleration time-history data (amplitude, α(ω)) and the frequency-weighted response spectrum (F.W. amplitude, α(ω)), calculated by multiplying each frequency component by the frequency weighting function (W_f), are presented in Fig. 12 and Fig. 13.

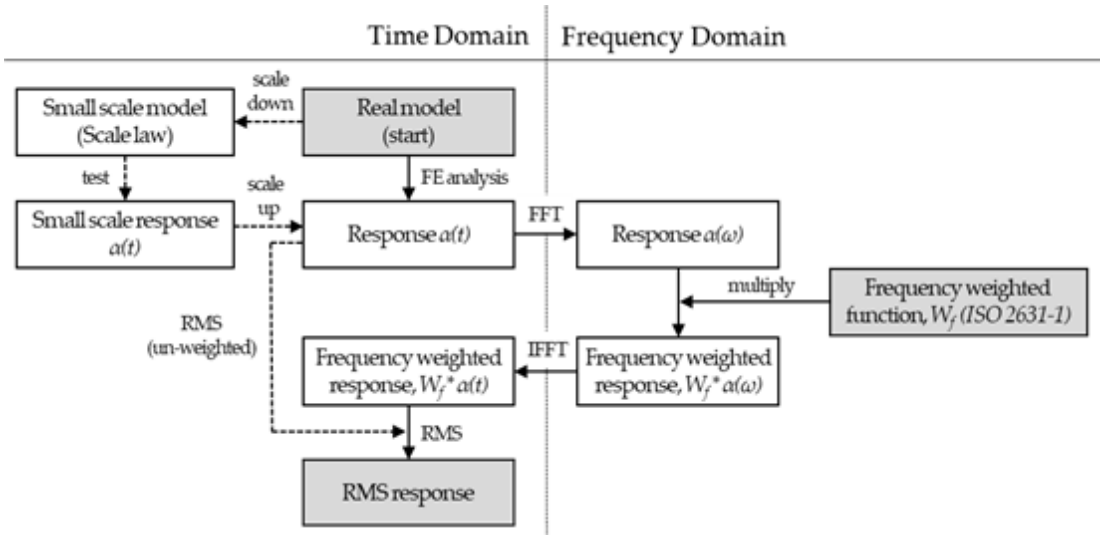

Figure 9. Process of frequency-weighted RMS acceleration

The motion periods of the floating body were found to be similar to the wave periods, with distributions of 0.18 Hz (5.5 s) for the 1-year return period and 0.14 Hz (7.0 s) for the 100-year return period. Consequently, the motion periods of the floating body are distributed around 0.16 Hz (6.25 s),

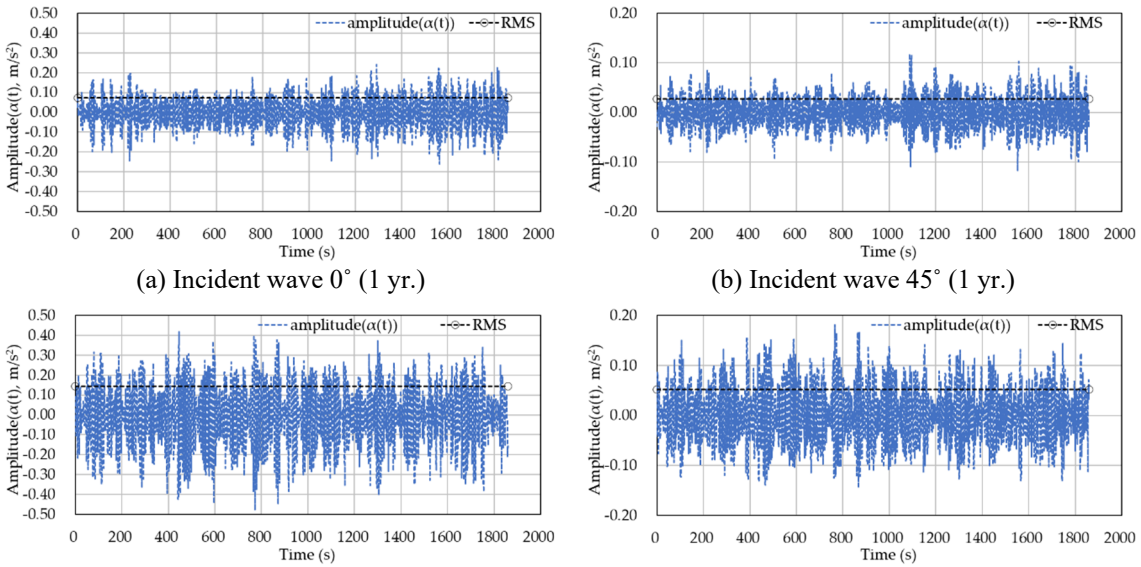

(a) Incident wave 0˚ (1 yr.) (b) Incident wave 45˚ (1 yr.)

(c) Incident wave 0˚ (100 yr.) (d) Incident wave 45˚ (100 yr.)

Figure 10. Measured acceleration: A model, M1(ACC.1)

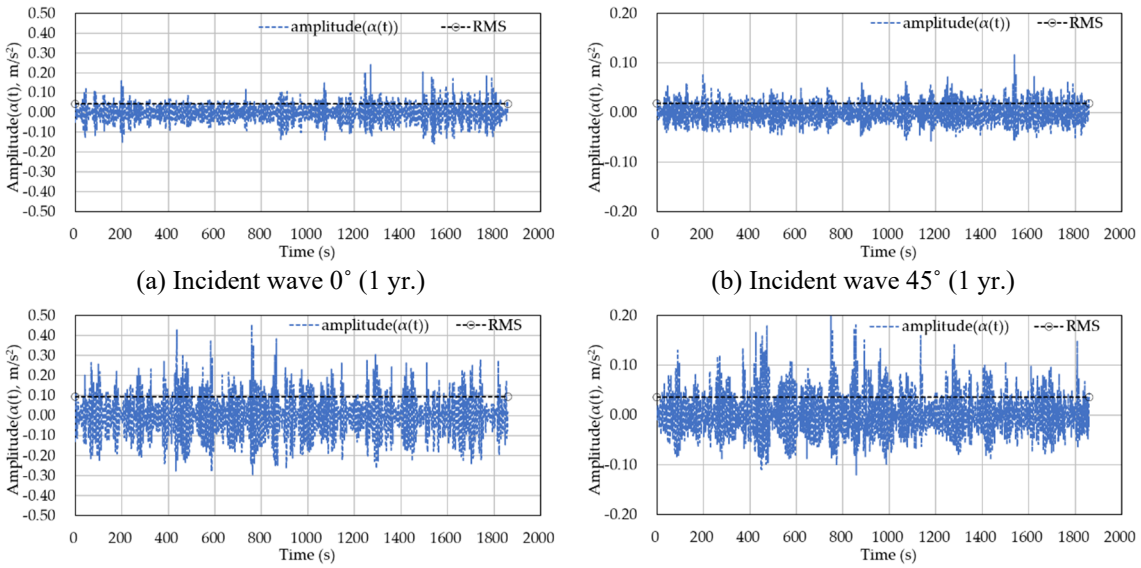

(a) Incident wave 0˚ (1 yr.) (b) Incident wave 45˚ (1 yr.)

(c) Incident wave 0˚ (100 yr.) (d) Incident wave 45˚ (100 yr.)

Figure 11. Measured acceleration: B model, M1(ACC.1)

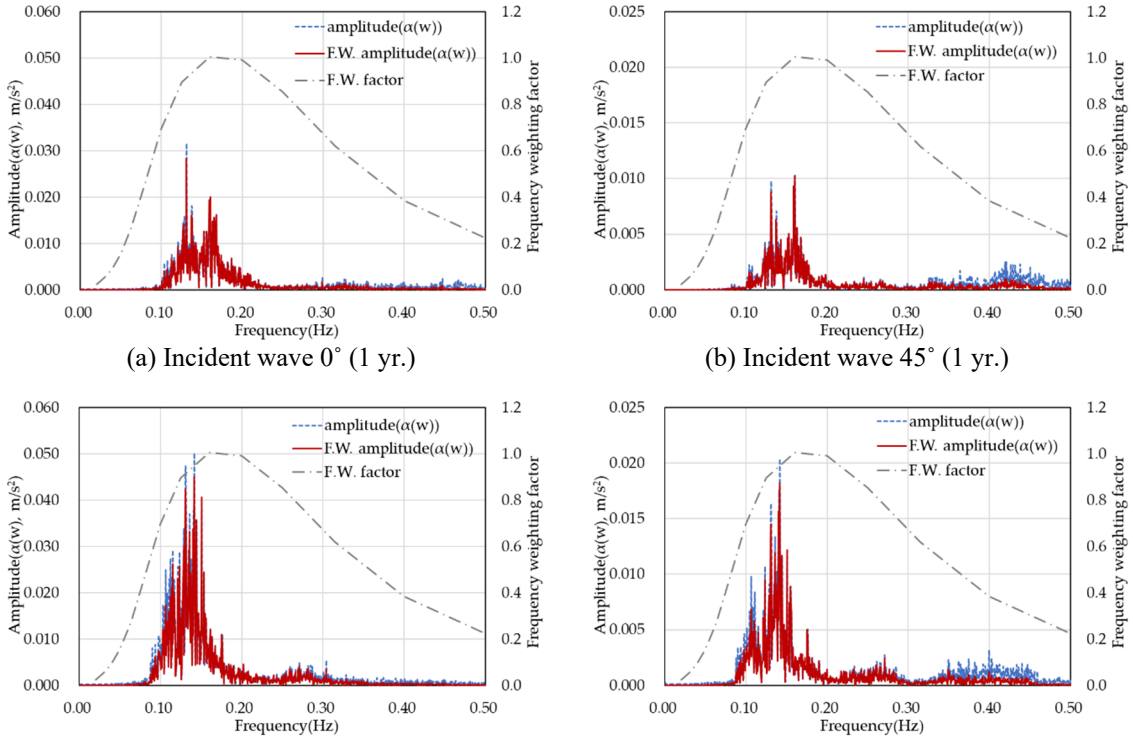

(a) Incident wave 0˚ (1 yr.) (b) Incident wave 45˚ (1 yr.)

(c) Incident wave 0˚ (100 yr.) (d) Incident wave 45˚ (100 yr.)

Figure 12. Response spectrums: A model, M1(ACC.1)

Table 4. Vertical accelerations: RMS, m/s^2

Items		1 yr. (IR-2)				100 yr. (IR-7)			
		Incident wave 0˚		Incident wave 45˚		Incident wave 0˚		Incident wave 45˚	
		RMS_Un	RMS_FW	RMS_Un	RMS_FW	RMS_Un	RMS_FW	RMS_Un	RMS_FW
A (M1)	MAX	0.261	0.228	0.119	0.083	0.480	0.408	0.181	0.146
	RMS	0.073	0.068	0.028	0.024	0.144	0.128	0.052	0.045
		-	(0.94)	-	(0.88)	-	(0.89)	-	(0.87)
B (M1)	MAX	0.240	0.144	0.116	0.061	0.455	0.262	0.198	0.103
	RMS	0.044	0.041	0.018	0.016	0.094	0.083	0.036	0.032
		-	(0.93)	-	(0.89)	-	(0.88)	-	(0.87)
B/A (RMS)		0.61	0.61	0.65	0.66	0.65	0.64	0.69	0.70

which is the frequency most strongly associated with human motion sickness. As a result, the frequency-weighted response spectrum (red line) and the un-weighted response spectrum (blue line) exhibit similar distributions, indicating that the reduction effect of the frequency weighting factor relative to the un-weighted case is minimal.

The time-history responses obtained through the inverse FFT of the frequency-weighted response spectrum, together with their RMS values (frequency-weighted RMS acceleration), are presented in Fig.

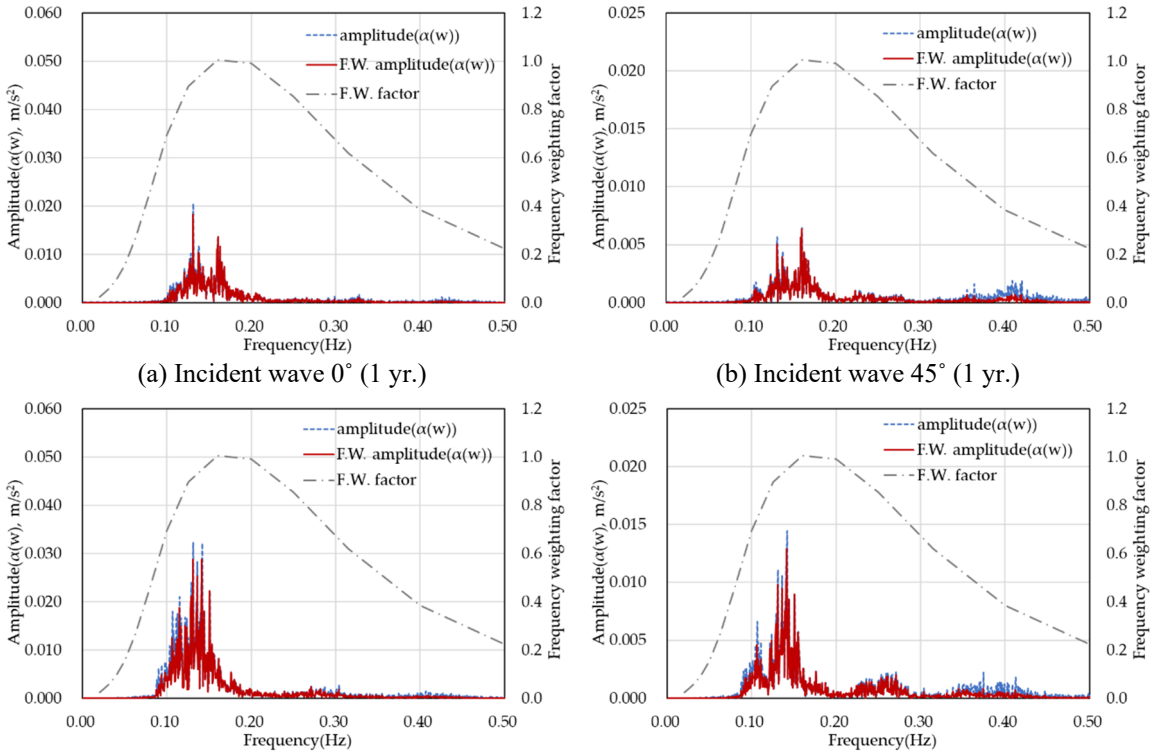

(a) Incident wave 0˚ (1 yr.) (b) Incident wave 45˚ (1 yr.)

(c) Incident wave 0˚ (100 yr.) (d) Incident wave 45˚ (100 yr.)

Figure 13. Response spectrums: B model, M1(ACC.1)

14, 15 and Table 4. The evaluation results show that the RMS acceleration of Model A under the 1-year return period wave load ranged from approximately 0.028 to 0.073 m/s², with the frequency-weighted RMS acceleration corresponding to about 88-94% levels of the un-weighted RMS acceleration. For Model B, the RMS acceleration under the 1-year return period wave load ranged from approximately 0.018 to 0.044 m/s², with the frequency-weighted RMS acceleration corresponding to about 89-93% levels of the un-weighted RMS acceleration.

The RMS acceleration of Model B, equipped with wave-dissipating modules, was about 61-66% levels of that of Model A, indicating that the vertical acceleration was reduced by approximately 34-39% due to the installation of wave-dissipating modules. This result demonstrates that the serviceability of the multi-unit floating body was improved.

3.2 Inclination

The serviceability evaluation indicators for inclination were assessed by calculating the maximum values and RMS values from the time-history data. The maximum values are related to the stable operation of the topside facilities (e.g., prevention of malfunction or failure) [3, 5], while the RMS values are associated with human activity [4]. Inclination refers to pitch and roll in the vertical direction, and when both components occur simultaneously, the combined value is calculated using the Square Root of the Sum of Squares (SRSS) method, as shown in Eq. (1) [7].

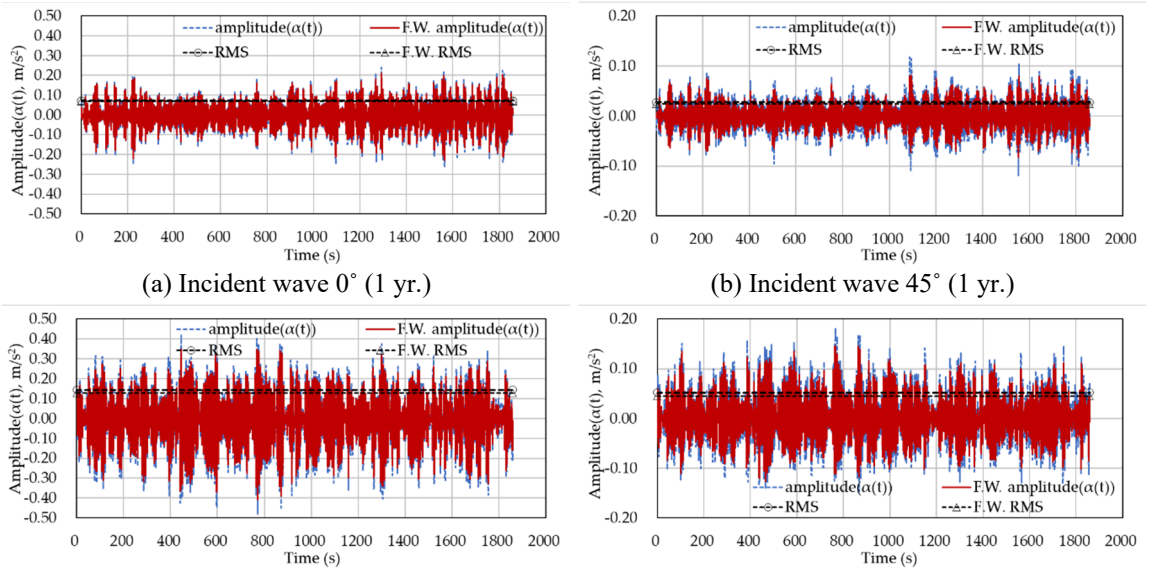

(a) Incident wave 0˚ (1 yr.) (b) Incident wave 45˚ (1 yr.)

(c) Incident wave 0˚ (100 yr.) (d) Incident wave 45˚ (100 yr.)

Figure 14. Frequency-weighted RMS acceleration: A model, M1(ACC.1)

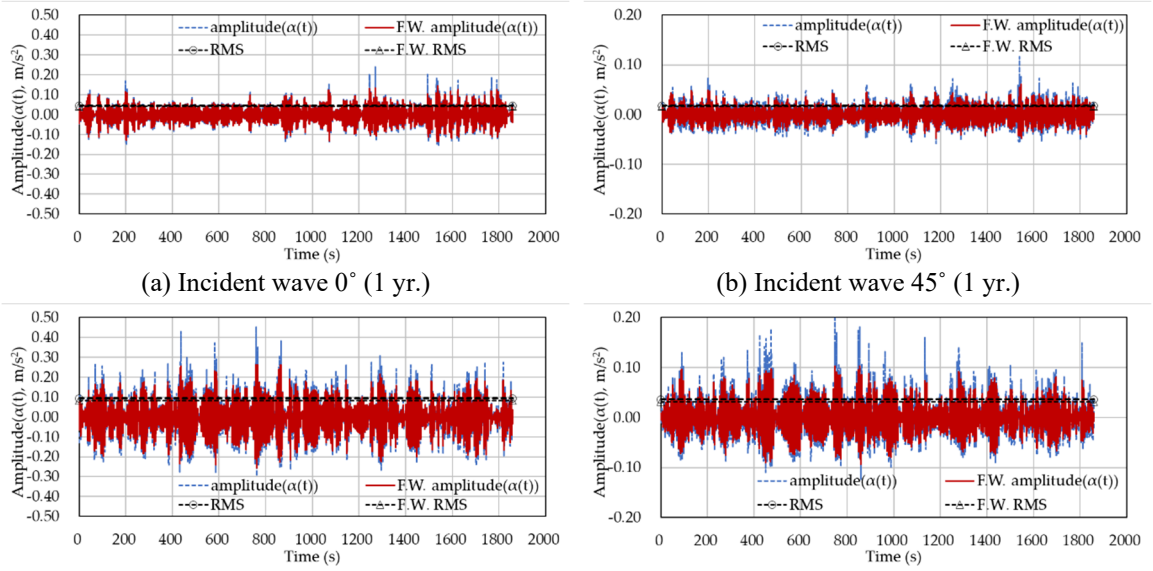

(a) Incident wave 0˚ (1 yr.) (b) Incident wave 45˚ (1 yr.)

(c) Incident wave 0˚ (100 yr.) (d) Incident wave 45˚ (100 yr.)

Figure 15. Frequency-weighted RMS acceleration: B model, M1(ACC.1)

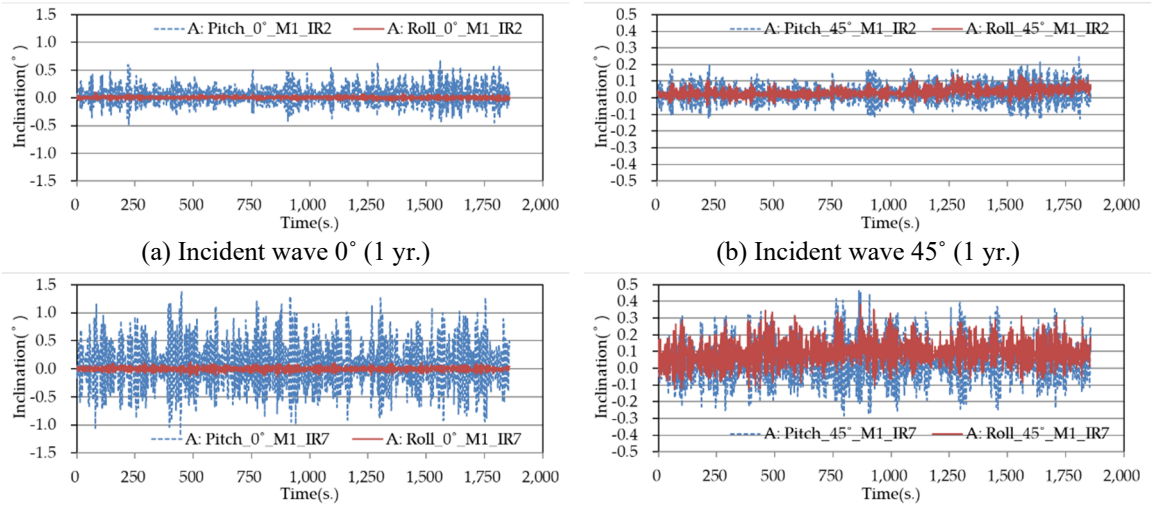

(a) Incident wave 0° (1 yr.) (b) Incident wave 45° (1 yr.)

(c) Incident wave 0° (100 yr.) (d) Incident wave 45° (100 yr.)

Figure 16. Measured pitch & roll angle: A model

Table 5. MAX and RMS inclination (°)

Items		1 yr. (IR-2)		100 yr. (IR-7)	
		Incident wave 0°	Incident wave 45°	Incident wave 0°	Incident wave 45°
A_M1	MAX	0.666	0.279	1.376	0.578
	RMS	0.172	0.077	0.423	0.178
A_M3	MAX	0.127	0.156	0.323	0.399
	RMS	0.042	0.060	0.104	0.126
B_M1	MAX	0.456	0.175	0.985	0.415
	RMS	0.117	0.050	0.293	0.104
B_M3	MAX	0.088	0.101	0.256	0.269
	RMS	0.030	0.044	0.081	0.096

$$R_{rot}(t) = SRSS = \sqrt{(R_{pitch}(t))^2 + (R_{roll}(t))^2}\,, \tag{1}$$

where, $R_{rot}(t)$ represents the total inclination, $R_{pitch}(t)$ represents the pitch inclination, and $R_{roll}(t)$ represents the roll inclination, respectively.

At the serviceability evaluation position, M1 unit, the inclination time-history data measured for Models A and B are shown in Fig. 16 and Fig. 17, respectively, while the SRSS time histories of pitch and roll are presented in Fig. 18, 19 and Table 5. The evaluation results indicate that, under the 1-year return period wave load, the inclination (maximum) of Model A ranged from approximately 0.28° to 0.67°, and the inclination (RMS) ranged from approximately 0.08° to 0.17°. For Model B, the inclination (maximum) ranged from approximately 0.18° to 0.46°, and the inclination (RMS) ranged from approximately 0.05° to 0.12°.

The inclination of Model B, equipped with wave-dissipating modules, was about 58-79% levels of that of Model A, indicating a reduction of approximately 21-42% in inclination due to the installation of wave-dissipating modules. This demonstrates that the serviceability of the multi-unit floating body was improved.

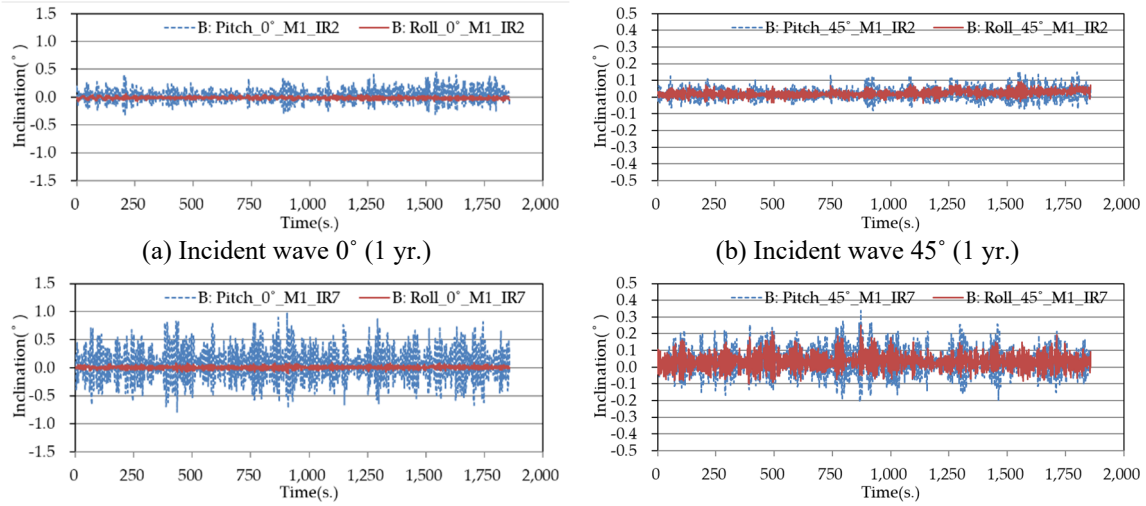

(a) Incident wave 0° (1 yr.) (b) Incident wave 45° (1 yr.)

(c) Incident wave 0° (100 yr.) (d) Incident wave 45° (100 yr.)

Figure 17. Measured pitch & roll angle: B model

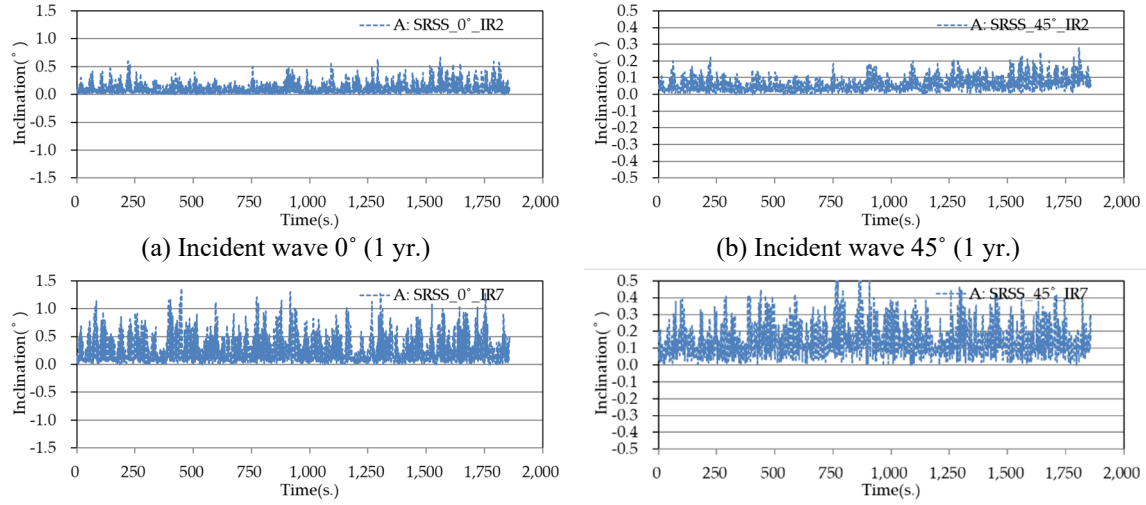

(a) Incident wave 0° (1 yr.) (b) Incident wave 45° (1 yr.)

(c) Incident wave 0° (100 yr.) (d) Incident wave 45° (100 yr.)

Figure 18. SRSS of pitch & roll angle: A model

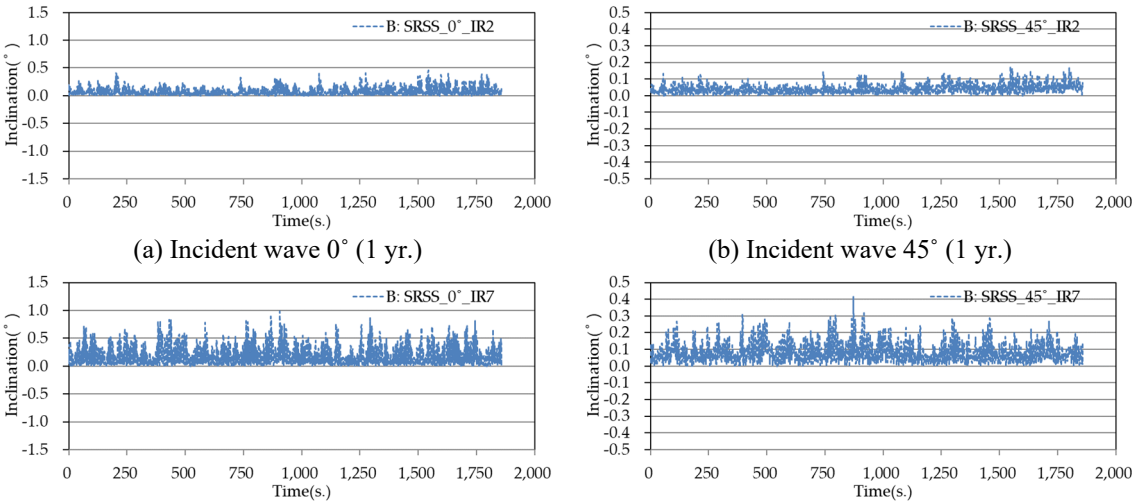

(a) Incident wave 0° (1 yr.) (b) Incident wave 45° (1 yr.)

(c) Incident wave 0° (100 yr.) (d) Incident wave 45° (100 yr.)

Figure 19. SRSS of pitch & roll angle: B model

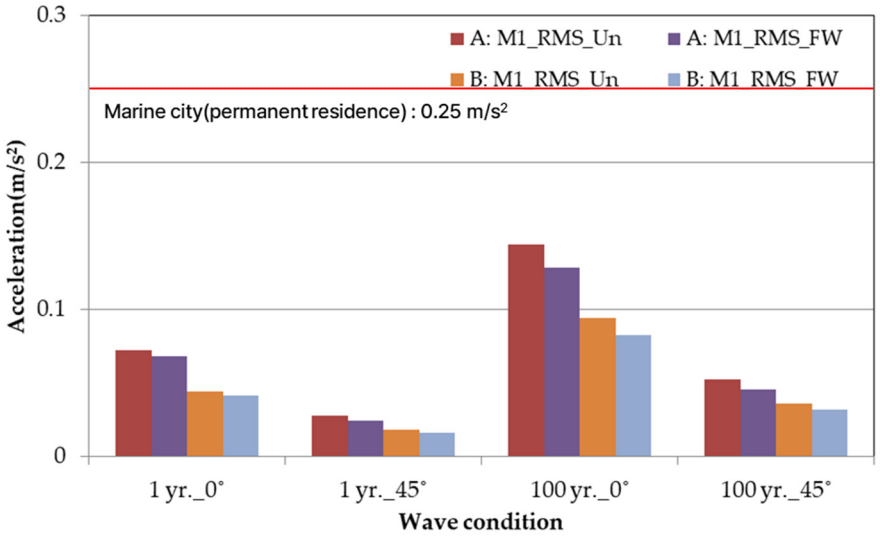

Figure 20. Summary of vertical acceleration evaluation

3.3 Summary

By analyzing various guidelines [4, 6, 30] available for the classification of vertical acceleration as a serviceability indicator of floating bodies, the classification can be broadly divided into three groups. The criteria for classification are generally based on the duration of exposure. For example, in the case of human habitation, Group 1 (permanent residence, < 0.25 m/s²), Group 2 (temporary residence, < 0.50 m/s²), and Group 3 (short-term stay, < 1.00 m/s²) can be distinguished.

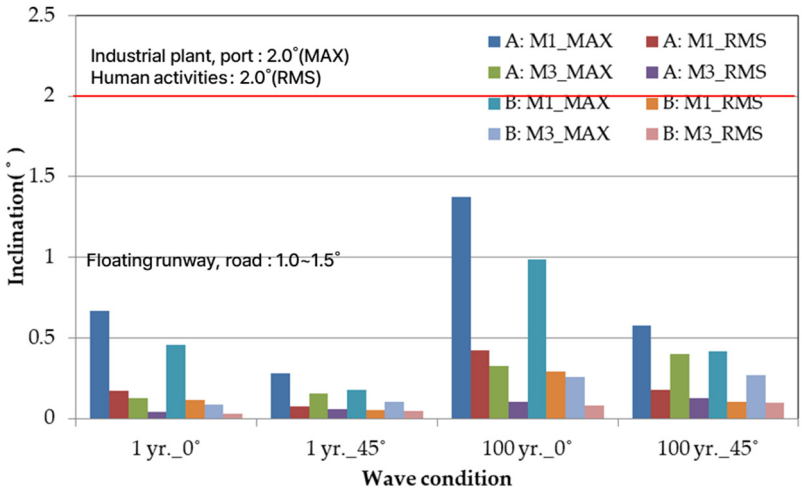

Figure 21. Summary of inclination evaluation

The evaluation results of vertical acceleration under various wave conditions (return periods and incident angles) are presented in Fig. 20. The results indicate that the vertical acceleration of the multi-unit floating infrastructure in this study reached a maximum of 0.073 m/s² under the 1-year return period wave load, corresponding to Group 1 (< 0.25 m/s²). This satisfies the performance target of a marine city for permanent human residence. Furthermore, under the 100-year return period wave load, the maximum vertical acceleration was 0.144 m/s², which also remained within Group 1 (< 0.25 m/s²).

By analyzing various guidelines [3, 4, 5] available for the classification of inclination as a serviceability indicator of floating bodies, the classification can be broadly divided into three groups. The criteria are determined according to the operational feasibility of the topside facilities. For cases requiring high safety levels, such as marine airports and marine roads, Group 1 (land-like flatness, < 1.0–1.5°) is applied. For industrial plants, where the prevention of equipment malfunction or failure is critical, or for ensuring human activity, Group 2 (high flatness, < 2.0°) is applied. For workspaces, where securing workability is the main objective, Group 3 (medium flatness, < 3.5°) is applied. In this context, maximum values should be applied to evaluate the stable operation of equipment, while RMS values should be applied to assess human activity and workability. The evaluation results of inclination under various wave conditions (return periods and incident angles) are presented in Fig. 21. Under the 1-year return period wave load, the multi-unit floating infrastructure exhibited a maximum inclination of 0.67° and an RMS inclination of 0.17°, both corresponding to Group 1 (< 1.0-1.5°). This satisfies the performance targets of a marine city, ensuring stable operation of topside equipment and meeting the criteria for human activity. Furthermore, under the 100-year return period wave load, the maximum inclination was 1.38° and the RMS inclination was 0.42°, which also remained within Group 1 (< 1.0-1.5°).

4. Conclusions

This study experimentally evaluated the serviceability of multi-unit floating structures designed for marine city applications and verified the effect of wave-dissipating modules on motion

reduction. Serviceability indicators were defined as vertical acceleration and inclination (pitch and roll), reflecting both the stable operation of topside facilities and human activity and discomfort (motion sickness).

The experimental results demonstrated that the introduction of wave-dissipating modules significantly improved serviceability performance. Specifically, vertical RMS accelerations were reduced by approximately 34-39%, while pitch and roll inclinations decreased by 21-42%. These improvements were consistently observed not only under 1-year return period wave conditions but also under extreme 100-year return period waves, thereby confirming the reliability of the proposed design.

This study shows that wave-dissipating modules serve as an effective design strategy to enhance the motion performance of floating structures, improving both the operational stability of topside facilities and the habitability of marine city environments. Furthermore, by applying ergonomics-based serviceability criteria such as ISO 2631-1:1997, the evaluation framework can be extended beyond industrial facilities to human-oriented offshore infrastructures, reflecting the dual requirements of technical stability and human-oriented serviceability in marine city contexts.

In conclusion, this study experimentally demonstrated that multi-unit floating structures equipped with wave-dissipating modules can achieve improved serviceability under realistic sea conditions. These findings are expected to make an important contribution to the development of next-generation offshore infrastructures, such as marine cities and offshore renewable energy hubs, where both technical stability and human-oriented serviceability must be simultaneously ensured. Future research should further establish the applicability of this approach through additional analyses under diverse sea conditions.

Acknowledgements

This work is supported by the Korea Agency for Infrastructure Technology Advancement (KAIA) grant funded by the Ministry of Land, Infrastructure, and Transport (Grant RS-2023-00250727), and the Korea Institute of Civil Engineering and Building Technology (KICT) grant funded by the Ministry of Science and ICT (Grant 20260157-001, Development of UAM floating vertiport design and construction technology).

References

1. Jeong, Y.J., Kim, J., Park, J.H., Kim, Y.T., Park, M.S. (2023). A study on serviceability recommendations for human activity-oriented floating structures. KSCE 2023 Convention, Yeosu, South Korea.
2. Jeong, Y.J., Park, M.S., Kim, Y.T., Kim, J. (2025). Experimental study on enhanced serviceability for human activities of floating structures with wave-dissipating modules. Journal of Marine Science and Engineering, 13(385). https://doi.org/10.3390/jmse13020385.
3. Japan Shipbuilding Society (2004), Structural design of very large floating structure. Japan.
4. Nordforsk (1987). Assessment of ship performance in a seaway, the Nordic co-operative project: seakeeping performance of ships. Nordic Co-operative Organization for Applied Research, Norway.
5. DNV-OS-J101 (2010). Design of offshore wind turbine structures. Det Norske Vertas, Oslo, Norway.
6. ISO 2631-1 (1997). Mechanical vibration and shock evaluation of human exposure to whole body vibration Part 1: general requirement. International Organization for Standardization, Switzerland.

7. Scheu, M., Matha, D., Schwarzkopf, M., Kolios, A. (2018). Human exposure to motion during maintenance on floating offshore wind turbines. Ocean Engineering, 165, 293-306. https://doi.org/10.1016/j.oceaneng.2018.07.016.
8. Schwarzkopf, M.A., Scheu, M.N., Altay, O., Kolios, A. (2018). Whole body vibration on offshore structures: an evaluation of existing guidelines for assessing low frequency motions. Proceedings of the 28th Int. Ocean and Polar Engineering Conference (ISOPE 2018), Sapporo, Japan. http://dspace.lib.cranfield.ac.uk/handle/ 1826/13617.
9. Marjanen, Y. (2010). Validation and improvement of the ISO 2631-1(1997) standard method for evaluating discomfort from whole-body vibration in multi-axis environment. Ph.D. Thesis, Loughborough University, Loughborough, UK.
10. Fang, C.C., Chan, H.S. (2007). An investigation on the vertical motion sickness characteristics of a high-speed catamaran ferry. Ocean Engineering, 34, 1909-1917. https://doi:10.1016/j.oceaneng.2007.04.001.
11. Kim, J., Welcome, D.E., Dong, R.G., Song, W.J., Hayden, C. (2007). Time-frequency characterization of hand-transmitted, impulsive vibrations using analytic wavelet transform. Journal of Sound and Vibration, 308, 98-111. https://doi:10.1016/j.jsv.2007.07.046.
12. Asua, E., Gutierrez-Zaballa, J., Mata-Carballeira, O., Andre-Ruiz, J., del Campo, I. (2022). Analysis of the motion sickness and the lack of comfort in car passengers. Applied Sciences, 12(3717). https://doi.org/10.3390/app12083717.
13. Sindre, M. (2012). Design criteria for offshore feed barge. Master thesis, NTNU, Trondheim, Norway.
14. Lee, J.I., Cho, J.H. (2001). Reflection characteristics of vertical slit caisson breakwater. Journal of Korean Society of Coastal and Ocean Engineers, 13(4), 263-272. https://doi.org/koix.ksci.re.kr/KISTI1.1003/ JNL.JAKO200111920885713.
15. Han, M., Wang, C.M. (2021). Modelling wide perforated breakwater with horizontal slits using hybrid-BEM method. Ocean Engineering, 222(108630). https://doi.org/10.1016/j.oceaneng.2021.108630.
16. Korea Institute of Construction Technology (2000). Wave reflection of perforated-wall caisson breakwaters, Goyang, South Korea.
17. Kim, J., Jeong, Y.J., Kim, Y.T. (2024). Frequency-domain analysis for motion of floating structures with perforated wall. Journal of Korean Society of Coastal and Ocean Engineers, 36(1), 1-10. https://doi.org/10.9765/KSCOE.2024.36.1.1.
18. Hur, D.S., Lee, W.D., Lee, H.W., Kim, I.C. (2010). The reflection characteristics of a perforated slit caisson with two chambers. Journal of Ocean Engineering and Technology, 24(1), 60-67.
19. Oh, S.H., Ji, C.H, Oh, Y.M., Jang, S.C., Lee, D.S. (2015). Comparison of maximum horizontal wave force acting on perforated caisson breakwater with single and double chamber. Journal of Korean Society of Coastal and Ocean Engineers, 26(5), 335-341. https://doi.org/10.9765/KSCOE.2014.26.5.335.
20. Xiao, L., Kou, Y., Tao, L., Yang, L. (2016). Comparative study of hydrodynamic performances of breakwaters with double-layered perforated walls attached to ring-shaped very large floating structures. Ocean Engineering, 111, 279-291. https://doi.org/10.1016/j.oceaneng.2015.11.007.
21. Wang, H., Yang, Y., Gua, Y., Lian, J. (2024). Influence of heave plate on the dynamic response of a 10MW semi-submersible floating platform. Journal of Marine Science and Engineering, 12(2156). https://doi.org/10.3390/jmse12122156.
22. Li, D., Gao, Y., Chen, J., Yi, C., Qi, L., Wen, B., Tian, X. (2025). Heave plate optimization for enhanced performance of semi-submersible wind turbine. Ships and Offshore Structures, Taylor & Francis. https://doi.org/10.1080/17445302.2025.2545908.
23. Turner, M., Wang, L., Thiagarajan, K., Robertson, A. (2023). Heave-plate hydrodynamic coefficients for floating offshore wind turbines: a compilation of data. Proceedings of the 5th Int. offshore wind technical conference (ASME). https://www.nrel.gov/docs/fy24osti/87275.pdf.
24. Chen, Z., Wang, Y., Dong, H., Zheng, B. (2012). Time-domain hydrodynamic analysis of pontoon-plate floating breakwater. Water Science and Engineering, 5(3), 291-303. https://doi.org/10.3882/j.issn.1674-2370.2012.03.005.

25. Carlos, L.P., Antonio, S.I. (2015). Hydrodynamic coefficients and pressure loads on heave plates for semi-submersible floating offshore wind turbines: a comparative analysis using large scale models. Renewable Energy, 81, 864-881. https://doi.org/10.1016/j.renene.2015.04.003.
26. Sudhakar, S., Nallayarasu, S. (2014). Hydrodynamic responses of spar hull with single and double heave plates in random waves. Int. Journal of Ocean System Engineering, 4(1), 1-18. https://doi.org/10.5574/IJOSE.2014.4.1.001.
27. Ana, B.B., Sergio, F.R., Adolfo, M.L., Enrique, M.F., Francisco, M.B., Julio, O.E., Jose, R.T., Cristina, S.G., Alvaro, V.P., Carlos, L.P., Antonio S.I. (2020). Scale effects on heave plates for semi-submersible floating offshore wind turbines: case study with a solid plain plate. Journal of Offshore Mechanics and Arctic Engineering, 142(3), 1-9. https://doi.org/10.1115/1.4045374.
28. Xu, J., Wang, C., Li, J., Tang, G., Yang, Y. (2024). Influence of damping plate size on pitch motion response of floating offshore wind turbine. Journal of Marine Science and Engineering, 12(1600). https://doi.org/10.3390/jmse12091600.
29. Ezoji, M., Shabakhty, N., Tao, L. (2022). Hydrodynamic damping of solid and perforated heave plate oscillating at low KC number based on experimental data: a review. International Journal of Ocean Engineering, 253(111247). https://doi.org/10.1016/j.oceaneng.2022.111247.
30. Rule Note NR 636 (2016). Comfort and health on-board offshore units. Bureau Veritas, Neuilly sur Seine Cedex, France.